JOURNAL OF MATERIALS SCIENCE 28 (1993) 4651–4659

Preparation and characterization of chromium oxide supported on zirconia

JONG RACK SOHN*, SAM GON RYU, MAN YOUNG PARK
Department of Industrial Chemistry, Engineering College, Kyungpook National University, Taegu 702-701, Korea

YOUNG IL PAE
Department of Chemistry, National Science College, Ulsan University, Ulsan 680-749, Korea

Chromium oxide/zirconia was prepared by dry impregnation of powdered $Zr(OH)_4$ with an aqueous solution of $(NH_4)_2CrO_4$. The characterization of prepared samples was performed using Fourier-transform infrared (FTIR) spectroscopy, X-ray photoelectron spectroscopy (XPS), X-ray diffraction (XRD), and differential thermal analysis (DTA), and by measurement of the surface area. The addition of chromium oxide to zirconia shifted the transitions of ZrO_2 from the amorphous to the tetragonal phase and from the tetragonal to the monoclinic phase to higher temperatures due to the strong interaction between chromium oxide and zirconia; and the specific surface area of the samples increased in proportion to the chromium-oxide content. Since the ZrO_2 stabilizes supported chromium oxide, chromium oxide was well dispersed on the surface of zirconia, and α-Cr_2O_3 was only observed at calcination temperatures above 1173 K. Upon the addition of only small amounts of chromium oxide (1 wt % Cr) to ZrO_2, both the acidity and acid strength of the samples increased remarkably, showing the presence of two kinds of acid sites on the surface of $CrOx/ZrO_2$ (Brönsted and Lewis acid sites).

1. Introduction

Supported chromium oxides are being used as catalysts for polymerization, hydrogenation, dehydrogenation, and oxidation–reduction reactions between environmentally important molecules such as CO and NO [1–5]. Recently, many efforts have involved the characterization of these samples in an attempt to find appropriate reaction mechanisms. Titrations to determine the oxidation state of the chromium when used in conjunction with infrared (i. r.) and electron-paramagnetic-resonance spectroscopy have provided much information on these matters. So far, however, they have been studied mainly in silica and alumina [6–8], and only a little work has studied the ZrO_2 support [9, 10].

Zirconia is an important material due to its interesting thermal and mechanical properties and so it has been investigated as a support and as a catalyst in recent years. Different papers have been devoted to the study of ZrO_2 catalytic activity in important reactions such as methanol and hydrocarbon synthesis from CO and H_2, or CO_2 and H_2 [11, 12], or alcohol dehydration [13, 14]. Zirconia has been extensively used as a support for metals or incorporated in supports to stabilize them or make them more resistant to sintering [15–17]. ZrO_2 activity and selectivity highly depend on the methods of preparation and the treatment used. In particular, in previous papers from this laboratory, it has been shown that NiO–ZrO_2 and ZrO_2 modified with sulphate ions are very active for acid-catalysed reactions, even at room temperature [18–20]. The high catalytic activities in the above reactions were attributed to the enhanced acidic properties of the modified catalysts, which originate from the inductive effect of S=O bonds of the complex formed by the interaction of oxides with the sulpha sulphate ion.

It is well known that the dispersion, the oxidation state, and the structural features of supported species may strongly depend on the support. The structure and physico-chemical properties of supported metal oxides are considered to be in different states to bulk metal oxides because of their interaction with the supports. This paper describes the preparation and characterization of chromium oxide supported on zirconia. The characterization of the samples was performed by means of FTIR, XRD, XPS and DTA, and by the measurement of the surface area.

2. Experimental procedure

2.1. $CrOx/ZrO_2$ preparation

The precipitate of $Zr(OH)_4$ was obtained by adding aqueous ammonia slowly into an aqueous solution of

* To whom all correspondence should be addressed.

zirconium oxychloride at room temperature with stirring until the pH of the mother liquor reached about 8. The precipitate thus obtained was washed thoroughly with distilled water until chloride ions were not detected, and then it was dried at room temperature for 12 h. The dried precipitate was powdered below 100 mesh.

The $CrOx/ZrO_2$ samples containing various chromium content were prepared by dry impregnation of powdered $Zr(OH)_4$ with an aqueous solution of $(NH_4)_2CrO_4$ followed by calcining at high temperatures for 1.5 h in air. This series of samples are denoted by their weight percentage of chromium. For example, 1–$CrOx/ZrO_2$ indicates the sample contains 1 wt % chromium.

2.2. Physico-chemical characterization

FTIR spectra were obtained in a heatable gas cell at room temperature using a Mattson Model GL 6030E spectrophotometer. The self-supporting $CrOx/ZrO_2$ wafers contained about 9 mg cm^{-2}. Prior to obtaining the spectra the samples were heated under vacuum at 673 ~ 773 K for 1.5 h.

The samples were checked in order to determine the structure of the support as well as that of chromium oxide by means of a Jeol Model JDX-8030 diffractometer, employing CuK_α (Ni filtered) radiation.

X-ray photoelectron spectra were obtained with a VG Scientific Model Escalab MK-II spectrometer. AlK_α and MgK_α were used as the excitation source, usually at 12 kV and 20 mA. The analysis chamber was at 10^{-7} Pa or better and the spectra of the samples, as fine powder, were analysed. However, to examine the redox behaviour of $CrOx/ZrO_2$, some samples were pressed onto a plate, treated with H_2 and O_2 in a separate gas cell, and transferred into a analysis chamber without exposure to air. Binding energies were referenced to the C_{1s} level at 285.0 eV.

DTA measurements were performed by a Dupon 2100 apparatus in flowing Ar (30 ml min^{-1}), and the heating rate was 5–10 K min^{-1}. For each experiment 30 ~ 50 mg of sample was used.

The specific surface area was determined by applying the Brunauer–Emmett–Teller (BET) method to the adsorption of N_2 at 77 K. Chemisorption of ammonia was also employed as a measure of the acidity of samples. The amount of chemisorption was obtained as the irreversible adsorption of ammonia [21].

3. Results and discussion

3.1. X-ray diffraction

The crystalline structure of $CrOx/ZrO_2$ calcined in air at different temperatures for 1.5 h was examined. Fig. 1 represents XRD patterns of ZrO_2 calcined in air at different temperatures. ZrO_2 was amorphous to XRD up to 573 K, with a two-phase mixture of the tetragonal and monoclinic forms at 623–873 K, and a monoclinic phase at 973 K. Three crystal structures of ZrO_2 (tetragonal, monoclinic and cubic phases) have been reported [22, 23].

On the other hand, in the case of supported chrom-

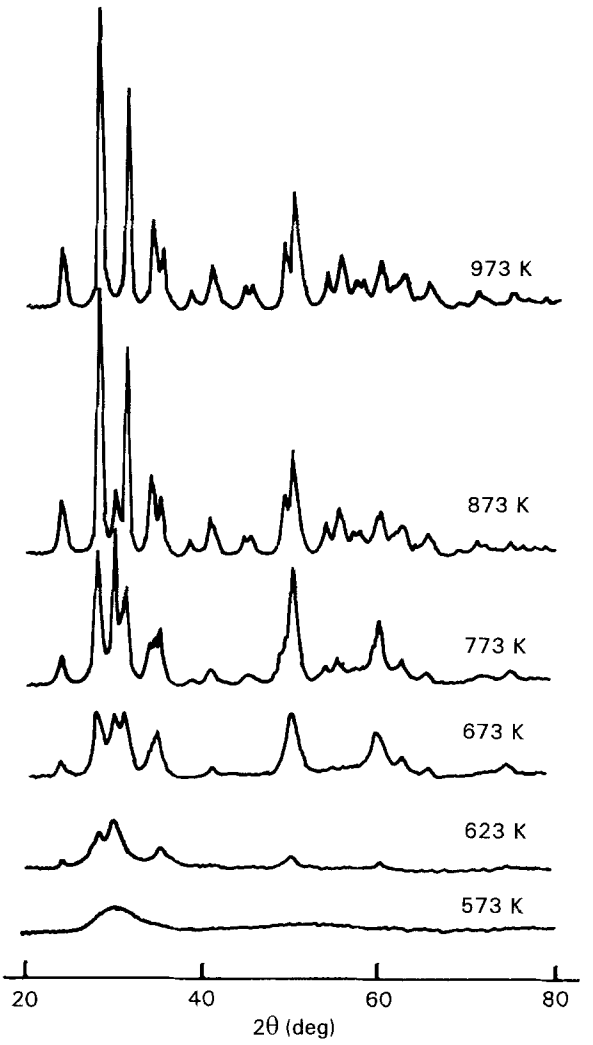

Figure 1 XRD patterns of ZrO_2 calcined at different temperatures for 1.5 h.

ium-oxide catalysts the crystalline structures of the samples were different from that of the support, ZrO_2. For 5–$CrOx/ZrO_2$, as shown in Fig. 2, ZrO_2 was amorphous up to 723 K. In other words, the transition temperature from the amorphous to tetragonal phase was 100 K higher than for pure ZrO_2. XRD data indicated a tetragonal phase of ZrO_2 at 773 K, a two-phase mixture of the tetragonal and monoclinic ZrO_2 forms at 873 ~ 1073 K, and a three-phase mixture of the tetragonal and monoclinic ZrO_2 forms and α-Cr_2O_3 at 1173 K. It is assumed that the strong interaction between chromium oxide and ZrO_2 hinders the transition of ZrO_2 from the amorphous to the tetragonal phase. The presence of chromium strongly influences the development of textural properties with temperature in comparison with pure ZrO_2. Moreover, for the sample of 10–$CrOx/ZrO_2$, the transition temperature from the amorphous to the tetragonal phase was higher by 200 K than that of pure ZrO_2 as shown in Fig. 3. That is, the higher the content of chromium, the higher is the transition temperature. These results are in agreement with those of DTA which will be described later. 10–$CrOx/ZrO_2$ was amorphous to XRD up to 773 K, with a tetragonal phase of ZrO_2 at 873–973 K, a two-phase mixture of the tetragonal and monoclinic forms at 1073 K, a

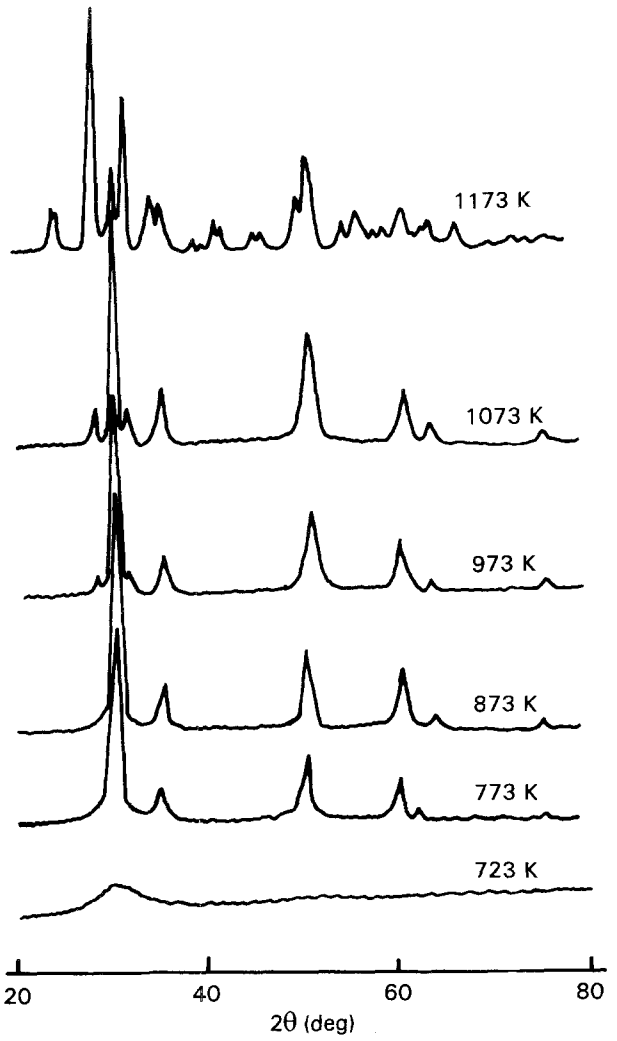

Figure 2 XRD patterns of 5–$CrOx/ZrO_2$ calcined at different temperatures for 1.5 h.

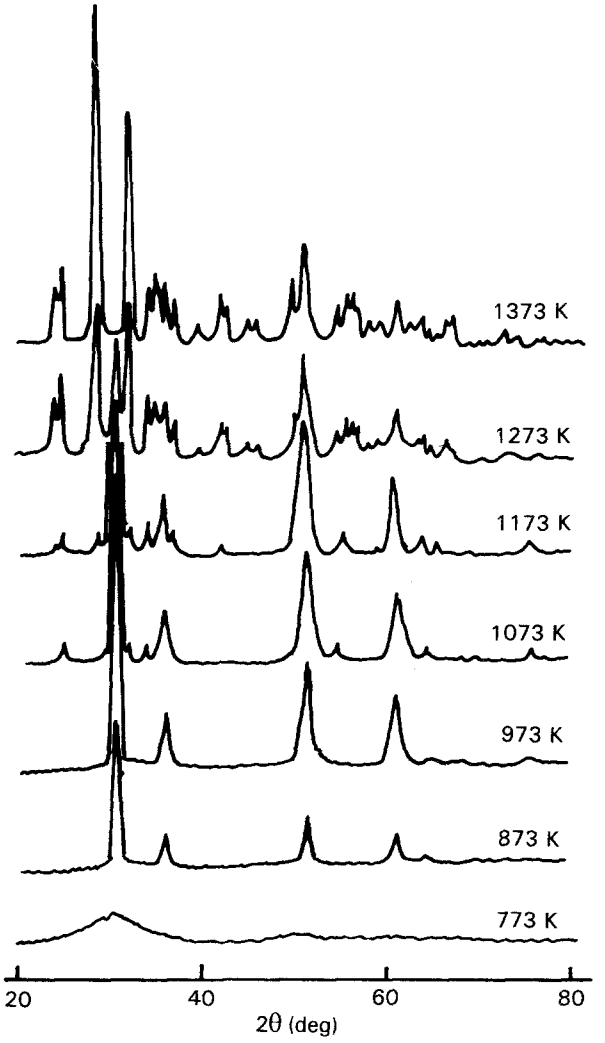

Figure 3 XRD patterns of 10–$CrOx/ZrO_2$ calcined at different temperatures for 1.5 h.

three-phase mixture of the tetragonal and monoclinic ZrO_2 forms and α-Cr_2O_3 at 1173~1273 K, and a two-phase mixture of the monoclinic ZrO_2 form and α-Cr_2O_3 at 1373 K. No phases of chromium oxide were observed up to a calcination temperature of 1073 K, indicating a good dispersion of chromium oxide on the surface of the ZrO_2 support due to the strong interaction between them. As shown in Figs 2 and 3, the α-Cr_2O_3 phase was observed only in the samples calcined above 1173 K, indicating that the ZrO_2 support stabilizes supported chromium oxide, and chromium oxide is well dispersed on the surface of ZrO_2 for calcination temperatures below 1173 K.

It is also of interest to examine the influence of chromium oxide on the transition temperature of ZrO_2 from the tetragonal to the monoclinic phase. Comparison of Figs 1–3 shows that the stabilization of the tetragonal phase is observed for $CrOx/ZrO_2$ samples. In view of the XRD patterns, the calcination temperatures at which the monoclinic phase is observed initially are 623 K for pure ZrO_2, 673 K for 1–$CrOx/ZrO_2$, 873 K for 5–$CrOx/ZrO_2$, and 973 K for 10–$CrOx/ZrO_2$. That is, the transition temperature increases with increasing chromium-oxide content. This can be also explained in terms of the delay of the transition from the tetragonal to the monoclinic phase due to the strong interaction between chromium oxide and zirconia, in analogy with the delay of the transition from the amorphous to the tetragonal phase described before.

3.2. Thermal analysis

In the XRD patterns, it was shown that the structure of $CrOx/ZrO_2$depended on the calcining temperature. To examine the thermal properties of the precursors of the samples more clearly, thermal analysis was carried out as illustrated in Fig. 4. For pure ZrO_2, the DTA curves show an endothermic peak in the temperature range 303~453 K due to water elimination, and a sharp and exothermic peak at 703~743 K due to ZrO_2 crystallization. In the case of $CrOx/ZrO_2$, an additional endothermic peak appeared at about 473 K due to the evolution of NH_3 decomposed from $(NH_4)_2CrO_4$. However, it is of interest to see the influence of chromium oxide on the phase transition of ZrO_2 from the amorphous to the tetragonal phase. As Fig. 4 shows, the exothermic peak due to the phase transition appears at about 723 K for pure ZrO_2, while for $CrOx/ZrO_2$ samples it is shifted to higher temperatures. The shift increases and the shape of peak becomes broad as the chromium content in-

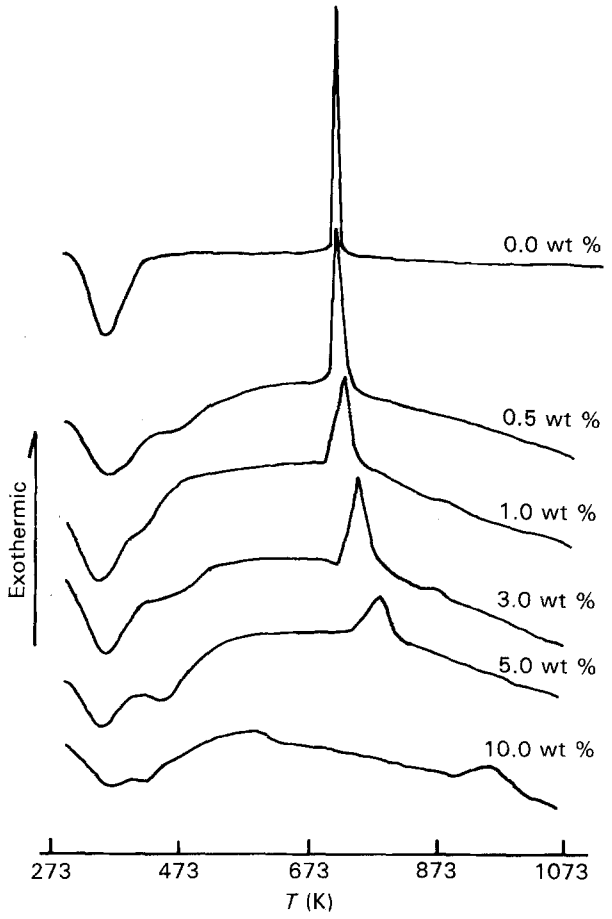

Figure 4 DTA curves of the precursors of the catalysts $Zr(OH)_4$ and $(NH_4)_2CrO_4/Zr(OH)_4$.

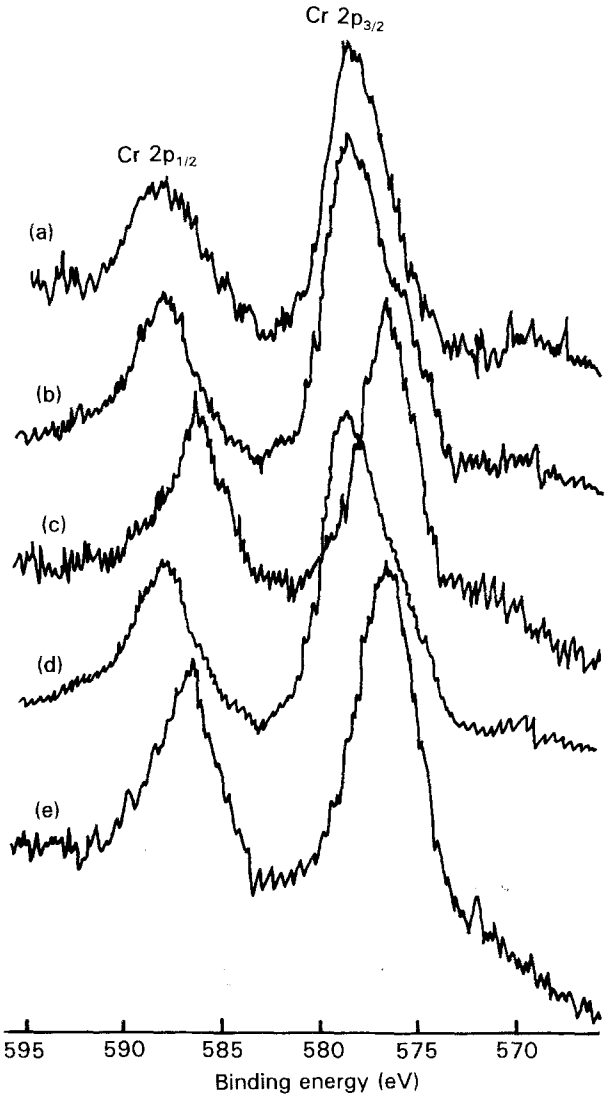

Figure 5 Cr 2p XPS of 3–$CrOx/ZrO_2$ treated under various conditions: (a) uncalcined sample, (b) sample calcined at 873 K, (c) after reduction of sample (b) with H_2 at 823 K, (d) after reoxidation of sample (c) with O_2 at 823 K, and (e) after reaction of sample (b) with *n*-hexane at 823 K.

creases. Consequently, for 10–$CrOx/ZrO_2$ the exothermic peak appears at 923 ~ 973 K. These results are in agreement with those of the XRD described above. It is relevant that the strong interaction between chromium oxide and zirconia delays the transition of ZrO_2 from the amorphous to the tetragonal phase. A similar observation has been made by Sohn and coworkers *et al.* [20, 24] for silica and sulphate ion additions.

3.3. X-ray photoelectron spectra

The difficulty in the study of supported chromium oxide comes from the simultaneous presence of oxidation states. Fig. 5 shows the Cr 2p spectra of 3–$CrOx/ZrO_2$ treated under various conditions. The shape of the peaks and the binding energies of the 2p electrons depend on the treatment conditions, indicating that the oxidation state of chromium varies with the treatment process.

To obtain further information on the oxidation state, the spectrum in the Cr $2p_3/_2$ region was analysed by appropriate curve fitting and the presence of two or three components was confirmed, as shown in Fig. 6. For the non-calcined and calcined samples, Cr $2p_{3/2}$ binding energies were obtained of 579.3 eV due to Cr(VI) and of 576.7 eV due to Cr(III). Cimino *et al.* [25] have measured Cr 2p binding energies for a variety of different chromium compounds. The corresponding Cr $2p_{3/2}$ binding energies for CrO_3 and Cr_2O_3 are 579.9 and 576.8 eV, respectively. Quantitative analysis for the chromium oxidation state was made and the results are listed in Table I. It is noted that the percentage of Cr(III) increases to some degree by the calcination at 873 K. However, the Cr(VI) concentration of the sample calcined at 873 K is quite large, of the order of 54% of the total Cr concentration, indicating that the ZrO_2 support stabilizes supported chromium oxide as follows:

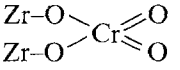

However, when sample (b) Fig. 6b was treated with H_2 at 823 K for 6 min, the Cr(VI) species was easily reduced to the Cr(III) species, as illustrated in Fig. 6c and Table I. Sample (c) was reoxidized with O_2 at 823 K for 6 min and its XPS result is shown in Fig. 6d. The Cr(VI)/Cr(III) ratio increased, which indicates that the reduction–oxidation process is reversible. One microlitre of *n*-hexane was reacted successively

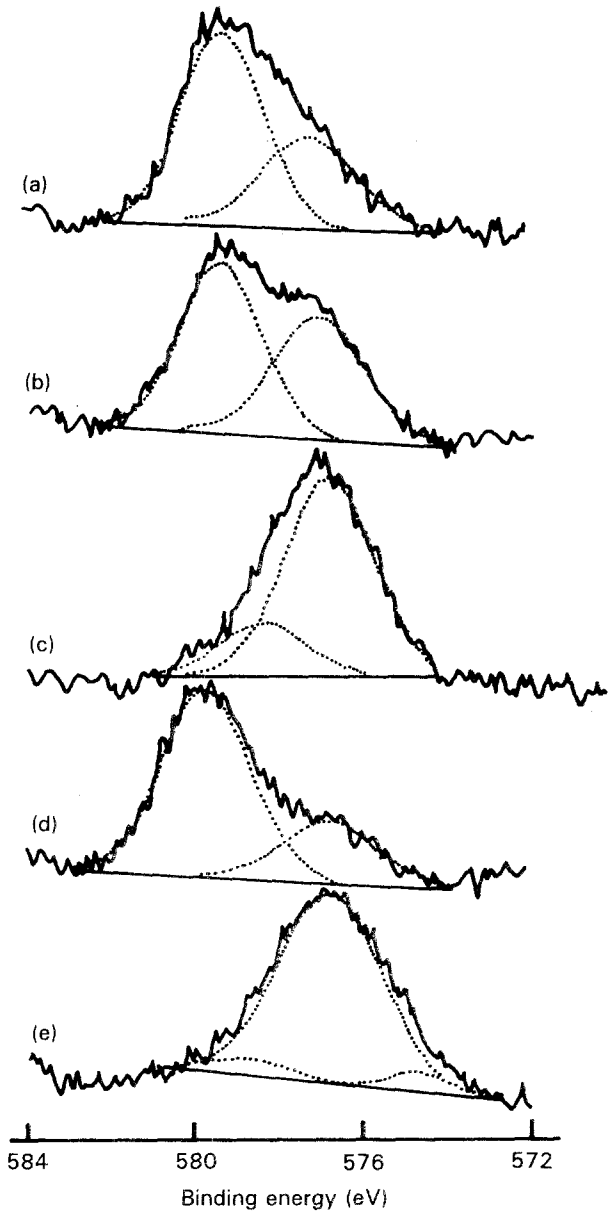

Figure 6 Cr $2p_{3/2}$ fitted XPS of 3–$CrOx/ZrO_2$ treated under various conditions: (a) uncalcined sample, (b) sample calcined at 823 K, (c) after reduction of sample (b) with H_2 at 823 K, (d) after reoxidation of sample (c) with O_2 at 823 K, and (e) after reaction of sample (b) with *n*-hexane at 823 K.

TABLE I Percentage of chromium species from the area of the fitted bands in the Cr $2p_{3/2}$ XPS region

Treatment condition	C^+ species (%)		
	Cr^{6+}	Cr^{3+}	Cr^0
Uncalcined sample	65	35	
Calcined in air at 873 K	54	46	
After reduction with H_2 at 823 K	19	81	
After oxidation with O_2 at 823 K	59	41	
After reaction with *n*-hexane at 823 K	3	89	7

ten times over the sample calcined at 873 K, where the reaction temperature was 823 K. XPS of the sample after this reaction is illustrated in Fig. 6e. The reaction results in the increase of the Cr(III) concentration. In this case a Cr $2p_{3/2}$ binding energy was also obtained

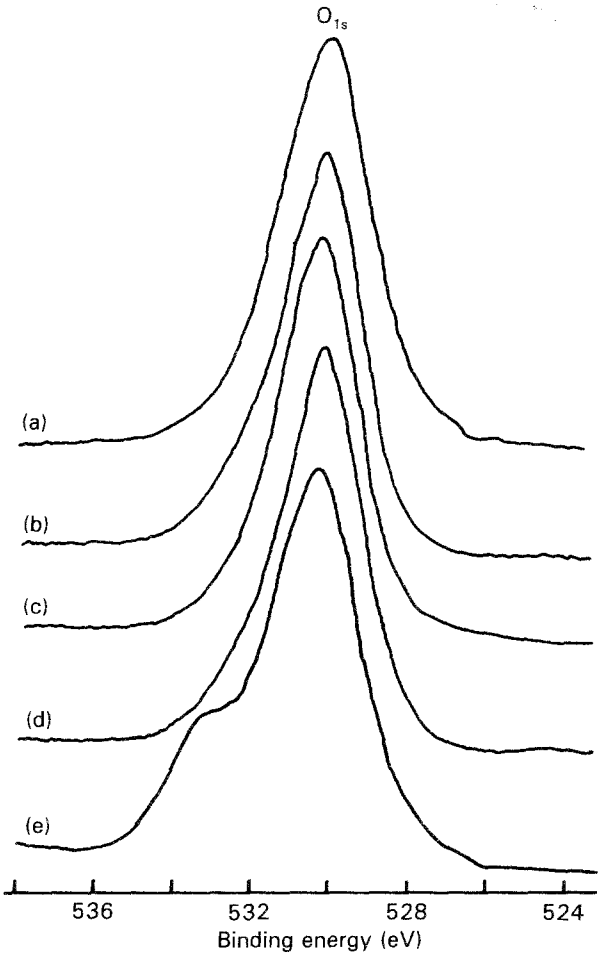

Figure 7 O_{1s} XPS of 3–$CrOx/ZrO_2$ treated under various conditions: (a) uncalcined sample, (b) sample calcined at 873 K, (c) after reduction of sample (b) with H_2 at 823 K, (d) after reoxidation of sample (c) with O_2 at 823 K, (e) after reaction of sample (b) with *n*-hexane at 823 K.

of 574.7 eV and assigned to chromium metal [26]. This again suggests reduction from Cr(VI) to Cr(III) or Cr(0) by *n*-hexane.

Fig. 7 shows the O_{1s} spectra of 3–$CrOx/ZrO_2$ treated under various conditions. In all the spectra the O_{1s} peak at a lower binding energy, 529.2 eV corresponds to lattice oxide ions [27]. However, for the sample reacted with *n*-hexane the O_{1s} peak at a higher binding energy, 531 eV, appeared. This peak can be attributed to a carbonate species formed during the catalytic reaction of *n*-hexane. Recently Gonzalez-Elipe *et al.* [27] have dealt with the characterization by XPS of the surface state of some metal oxides. In their work a second O_{1s} peak, appearing at the high binding-energy side of the main peak, corresponding to the oxide anions, has been attributed to carbonate species.

3.4. I. r. spectra

Fig. 8 shows the i. r. spectra of 1–$CrOx/ZrO_2$ treated under various conditions. After evacuation at 773 K for 1 h, three bands at 1032, 1018 and 920 cm^{-1} were observed. The doublet at 1032 and 1018 cm^{-1} is assigned to the asymmetric and symmetric stretching modes, respectively, of surface chromates [9]. The

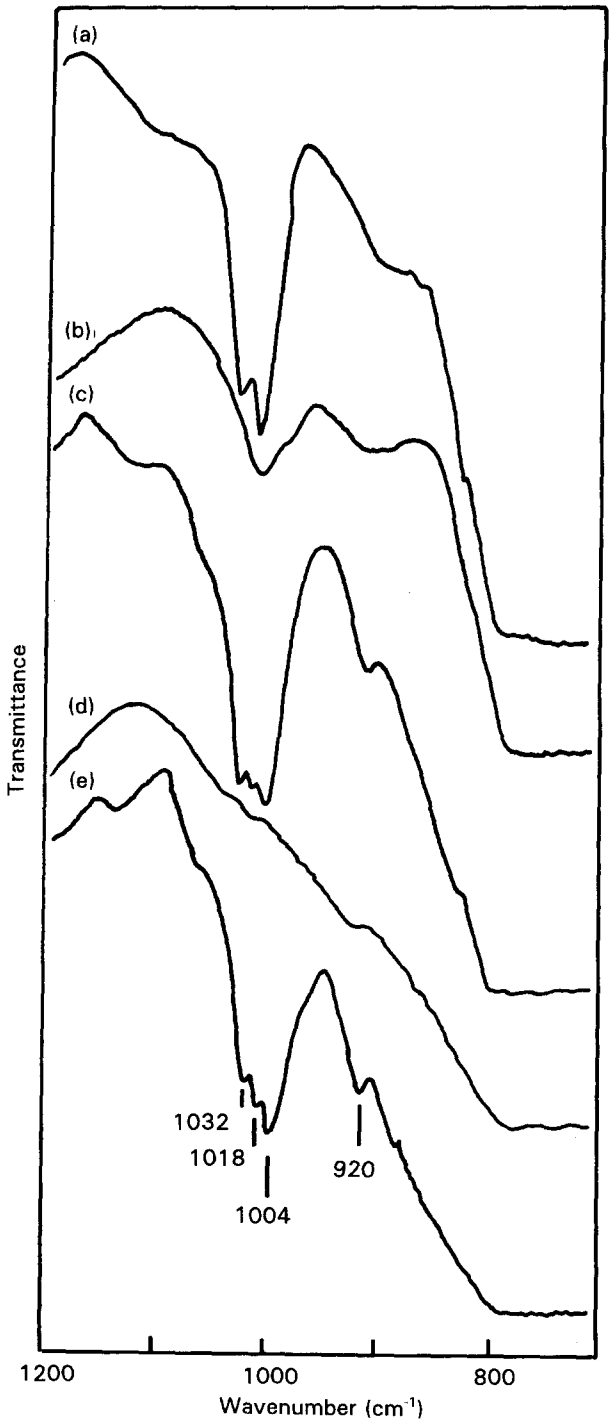

Figure 8 I. r. spectra of 1-$CrOx/ZrO_2$ treated under various conditions: (a) after evacuation at 773 K for 1 h, (b) after evacuation at 773 K for 2 h, (c) after oxidation of sample (b) with O_2 (6.6 kPa) at 773 K for 1 h, (d) after reduction of sample (c) with CO (6.6 kPa) at 773 K for 0.5 h and (e) after reoxidation of sample (d) with O_2 (6.6 kPa) at 773 K for 0.5 h.

broad band around 900 cm^{-1} is typical of chromium–oxygen groups of a lower double-bond character. However, upon evacuation at 773 K for 2 h the intensities of the doublet bands decreased remarkably due to the removal of surface oxygen. Reoxidation of sample (b) in Fig. 8 was performed by the addition of O_2 (6.6 kPa) at 773 K for 0.5 h and then the i. r. spectrum was taken at room temperature (Fig. 8c). Heating in oxygen at 773 K nearly restored the situation observed in Fig. 8a and an additional band at 1004 cm^{-1} assigned to Cr=O species was observed. The weak and sharp band at 920 cm^{-1} can be interpreted as due to the blue shift of the Zr–O–Cr mode caused by Cr oxidation. Upon reduction of the oxidized sample (c) in Fig. 8 with CO at 773 K, the intensities of all the bands in the range 1100–900 cm^{-1} decreased as shown in Fig. 8d. Upon introduction of O_2 (6.6 kPa) to the sample reduced with CO and on heating at 773 K for 0.5 h, the bands at 1032, 1018, 1004 and 920 cm^{-1} were also recovered. Complete reversibility was observed after reduction–oxidation processes and these results are in good agreement with those of XPS described above.

3.5. Surface properties of the $CrOx/ZrO_2$ catalyst

It is necessary to examine the effect of chromium oxide on the surface properties of $CrOx/ZrO_2$, that is, specific surface area, acidity, and acid strength. The specific surface areas of samples calcined at 873 K for 1.5 h are plotted as a function of chromium content in Fig. 9. The presence of chromium oxide strongly influences the surface area in comparison with the pure ZrO_2. The specific surface areas of the $CrOx/ZrO_2$ samples are much larger than those of pure ZrO_2 calcined at the same temperature, showing that surface area increases gradually with increasing chromium content. It seems likely that the strong interaction between chromium oxide and ZrO_2 protects catalysts from sintering. The dependence of this anti-sintering effect on chromium oxide content is clear from Fig. 9. These results are correlated with the fact that the transition temperature of ZrO_2 from the amorphous to the tetragonal phase increases with increasing chromium-oxide content in DTA experiments. These results are also in agreement with those of the phase transition of ZrO_2 observed in XRD patterns as illustrated in Figs 1–3.

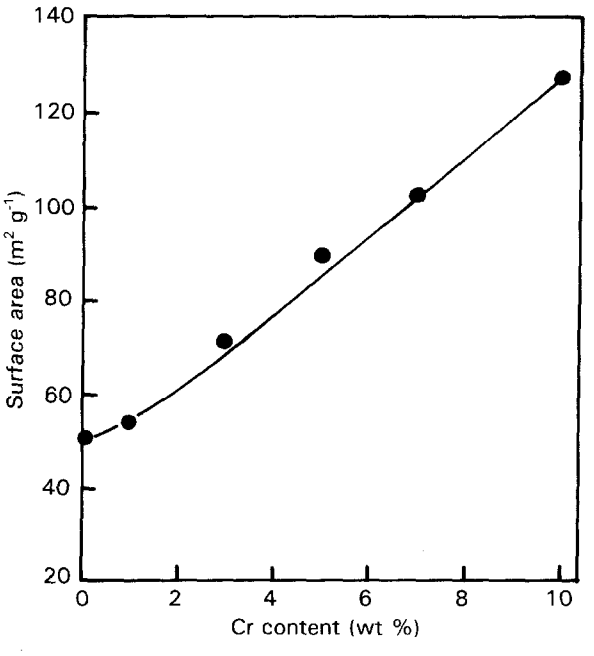

Figure 9 Variation of surface area of $CrOx/ZrO_2$, calcined at 873 K, with chromium content.

In addition to chromium-oxide content, calcination temperature influences the surface-area value. Pure ZrO_2 and some $CrOx/ZrO_2$ samples were subjected to calcining in air at a given temperature, and the results obtained are plotted in Fig. 10 as a function of calcination temperature. The anti-sintering effect of chromium oxide is greater at lower calcination temperatures than at higher temperatures. As illustrated in Fig. 10, the difference in surface area between pure ZrO_2 and $CrOx/ZrO_2$ calcined at 1173 K is very small compared with the cases of samples calcined at lower temperatures. For the $CrOx/ZrO_2$ samples, crystalline α-Cr_2O_3 was observed at the calcination temperature above 1173 K as described in the XRD results. Therefore, it seems likely that the small anti-sintering effect of chromium oxide at the calcination temperature of 1173 K is related to the formation of α-Cr_2O_3 and consequently to the weak interaction between α-Cr_2O_3 and zirconia.

The acid strength was examined by a colour-change method, using a Hammett indicator [28], when a powdered sample was added to an indicator dissolved in dried benzene. Since it was very difficult to observe the colour of indicators adsorbed on samples of high chromium-oxide content, a low percentage of chromium content (0.1 wt %) was used in this experiment. The results are listed in Table II. In this table, a plus sign indicates that the colour of the base form was changed to that of the conjugated acid form. ZrO_2 evacuated at 673 K for 1 h has an acid strength $Ho \leqslant -5.6$, while 0.1–$CrOx/ZrO_2$ was estimated to have a $Ho \leqslant -14.5$, indicating the formation of new acid sites stronger than those of single-oxide components. The acid strength of 0.1–$CrOx/ZrO_2$ oxidized with O_2 at 773 K was also found to be $Ho \leqslant -14.5$. Acids stronger than $Ho \leqslant -11.93$, which corresponds to

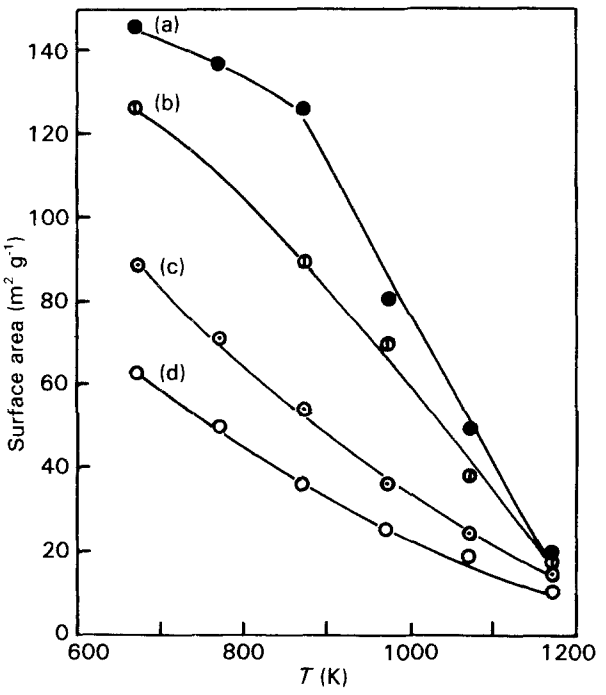

Figure 10 Variations of surface area for ZrO_2 and some $CrOx/ZrO_2$ samples against calcination temperature: (a) 10–$CrOx/ZrO_2$, (b) 5–$CrOx/ZrO_2$, (c) 1–$CrOx/ZrO_2$, (d) ZrO_2.

TABLE II Acid strength of 0.1–$CrOx/ZrO_2$ and ZrO_2

Hammett indicator	pKa value of indicator	$CrOx/ZrO_2$[a]	$CrOx/ZrO_2$[b]	ZrO_2
Dicinnamal-acetone	−3.0	+	+	+
Benzalaceto-phenone	−5.6	+	+	+
Anthraquinone	−8.2	+	+	−
Nitrobenzene	−12.4	+	+	−
2,4-Dinitro-fluorobenzene	−14.5	+	+	−

[a] Calcined in air at 873 K.
[b] Oxidized with O_2 at 773 K.

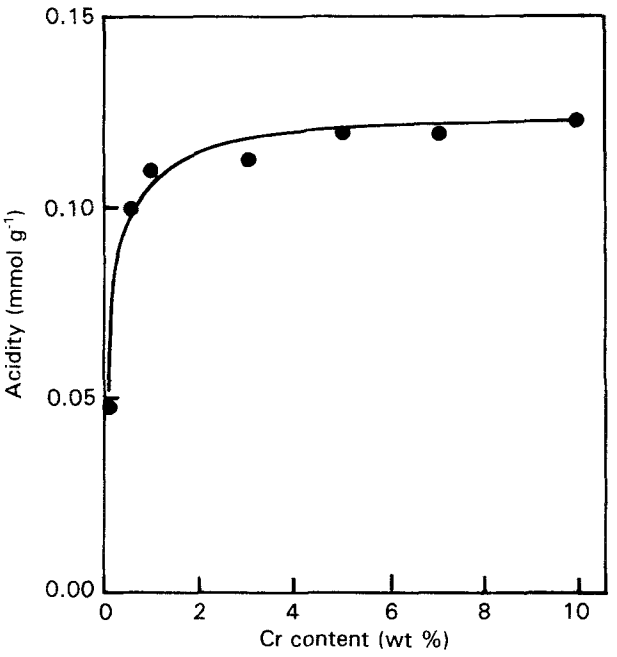

Figure 11 Acidity of $CrOx/ZrO_2$ plotted against chromium content.

an acid strength of 100% H_2SO_4, are superacidic [29]. Consequently, $CrOx/ZrO_2$ catalysts would be solid superacids. The superacidic property is attributed to the double-bond nature of the Cr=O in the complex formed by the interaction of ZrO_2 with chromate, in analogy with the case of ZrO_2 modified with sulphate ions [18–20].

The acidity of $CrOx/ZrO_2$, as determined by the amount of NH_3 irreversibly adsorbed at 503 K [21], is plotted as a function of the chromium content in Fig. 11. Although pure ZrO_2 showed an acidity of 0.05 meq g^{-1}, 1–$CrOx/ZrO_2$ resulted in a remarkable increase in acidity (0.1 meq g^{-1}). As shown in Fig. 11, the acidity increases abruptly upon the addition of 1 wt % chromium to ZrO_2, and then the acidity increases very gently with increasing chromium-oxide content. Many combinations of two oxides have been reported to generate acid sites on the surface [30–32]. The combination of ZrO_2 and $CrOx$ generates stronger acid sites and more acidity than the separate components. A mechanism for the generation of acid sites by mixing two oxides has been proposed by Itoh *et al.*

[30]. They suggest that the acidity generation is caused by an excess of a negative or positive charge in a model structure of a binary oxide related to the coordination number of a positive element and a negative element.

Infrared spectroscopic studies of pyridine adsorbed on solid surfaces have made it possible to distinguish between Brönsted and Lewis acid sites [33]. Fig. 12 shows the i.r. spectra of pyridine adsorbed on 1-$CrOx/ZrOx$ evacuated at 773 K for 1 h. There were peaks at 1443, 1483, 1497, 1554, 1580, 1595 and 1605 cm^{-1} comprising the vibrational modes of pyridine after evacuation at room temperature. Many peaks were weakened after evacuation at 523 K. Consequently, this set of disappeared absorption peaks can be assigned to hydrogen-bonded pyridine [34]. The bands at 1554 and 1497 cm^{-1} are the characteristic peaks of the pyridinium ion, which are formed on the Brönsted acid sites [35]. The other set of absorption peaks at 1443, 1483, 1580 and 1605 cm^{-1} are contributed by pyridine coordinatively bonded to Lewis acid sites. It is clear that both Brönsted and Lewis acid sites exist on the surface of $CrOx/ZrO_2$ samples calcined at 873 K.

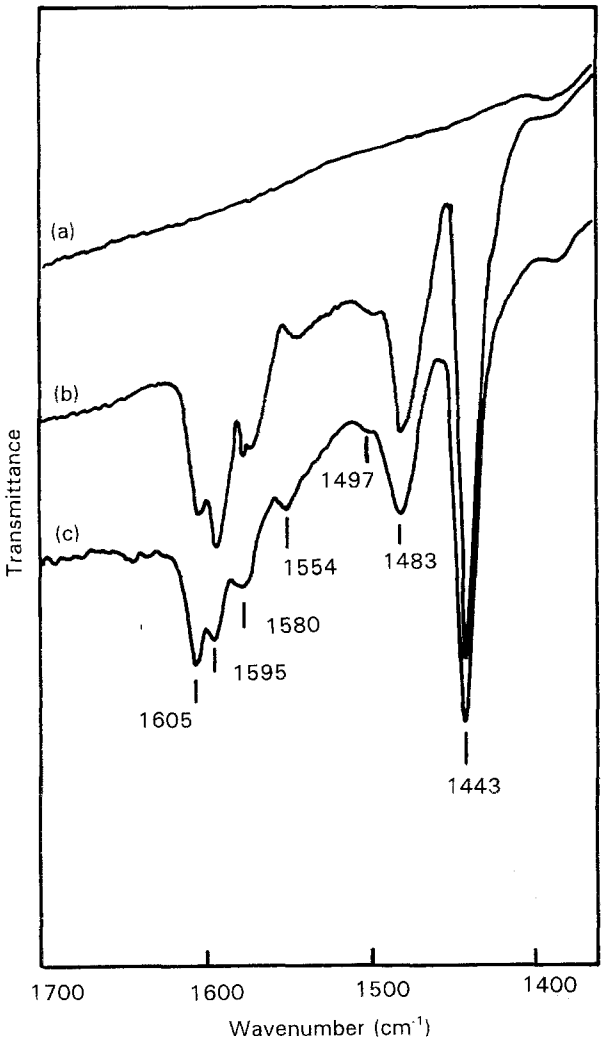

Figure 12 I. r. spectra of pyridine adsorbed on 1-$CrOx/ZrO_2$: (a) background of 1-$CrOx/ZrO_2$ after evacuation at 773 K for 1 h, (b) pyridine adsorbed on sample (a) followed by evacuation at room temperature for 1 h, (c) pyridine adsorbed on sample (a) followed by evacuation at 523 K for 1 h.

4. Conclusion

This paper has shown that a combination of FTIR, XPS, XRD and DTA can be used to perform the characterization of $CrOx/ZrO_2$ prepared by dry impregnation. The strong interaction between chromium oxide and zirconia influences the physico-chemical properties of prepared samples with temperature. The presence of chromium oxide delays the transitions of zirconia from amorphous and to tetragonal phase, and from tetragonal to monoclinic phase, and the specific surface area of samples increases in proportion to the chromium oxide content. The Cr(VI) concentration of 1-$CrOx/ZrO_2$ calcined at 873 K is quite large, of the order of 54% of the total Cr concentration, and α-Cr_2O_3 is observed only at calcination temperatures above 1173 K, indicating that the ZrO_2 support stabilizes supported chromium oxide, and chromium oxide is well dispersed on the surface of ZrO_2. By oxygen, hydrogen, carbon monoxide and *n*-hexane treatments, the reduction–oxidation behaviours from Cr(VI) to Cr(III) or vice versa are reversible, as evidenced by XPS and i.r. Upon the addition of only small amounts of chromium oxide (1 wt % Cr) to ZrO_2, both the acidity and acid strength of sample increases remarkably, showing the presence of two kinds of acid sites on the surface of $CrOx/ZrO_2$ – Brönsted and Lewis acid sites.

Acknowledgement

This paper was supported by the Research centre for Catalytic Technology, the Korea Science and Engineering Foundation.

References

1. J. P. HOGAN, *J. Polym. Sci.* **8** (1970) 2637.
2. D. L. MYERS and J. H. LUNSFORD, *J. Catal.* **99** (1986) 140.
3. A. CLARK, *Catal. Rev.* 3 (1969) 145.
4. C. GROENEVELD, P. P. M. M. WITTGEN, A. M. VAN KERSBERGEN, P. L. M. MESTROM, C. E. NUIJTEN and G. C. A. SCHUIT, *J. Catal.* **59** (1979) 153.
5. M. SHELEF, K. OTTO and H. GANDHI, *J. Catal.* **12** (1968) 361.
6. M. P. MCDANIEL, *Adv. Catal.* **33** (1985) 47.
7. G. GHIOTTI, E. GARRONE and A. ZECCHINA, *J. Mol. Catal.* **46** (1985) 61.
8. W. HILL and G. ÖHLMANN, *J. Catal.* **123** (1990) 147.
9. A. CIMINO, D. CORDISCH, S. FEBBRARO, D. GAZZOLI, V. INDOVINA, M. OCCHIUZZI and M. VALIGI, *J. Mol. Catal.* **55** (1989) 23.
10. T. YAMAGUCHI, M. TAN-NO and K. TANABE, "Preparation of Catalysts V" (Elsevier, Amsterdam, 1991) 567.
11. M. Y. HE and J. G. EKERDT, *J. Catal.* **90** (1984) 17.
12. T. MAEHASHI, K. MARUYA, K. DOMEN, K. AIKA and T. ONISHI, *Chem. Lett.* (1984) 747.
13. T. YAMAGUCHI, H. SASAKI and K. TANABE, *Chem. Lett.* (1973) 1017.
14. B. H. DAVIS and P. GANESAN, *Ind. Engng. Chem. Prod. Res. Dev.* **18** (1979) 191.
15. T. IIZUKA, Y. TANAKA and K. TANABE, *J. Catal.* **76** (1982) 1.
16. P. TURLIER, J. A. DALMON and G. A. MARTIN, *Stud. Surf. Sci. Catal.* **11** (1982) 203.
17. R. SZYMANSKI, H. CHARCOSSET, P. GALLEZOT, J. MASSARDIER and L. TOURNAYAN, *J. Catal.* **97** (1986) 366.
18. J. R. SOHN and H. J. KIM, *J. Catal.* **101** (1986) 428.

19. J. R. SOHN, H. W. KIM and J. T. KIM, *J. Mol. Catal.* **41** (1987) 379.
20. J. R. SOHN and H. W. KIM, *J. Mol. Catal.* **52** (1989) 361.
21. J. R. SOHN and A. OZAKI, *J. Catal.* **61** (1980) 29.
22. M. J. TORRALVO, M. A. ALARIO and J. SORIA, *J. Catal.* **86** (1984) 473.
23. A. CLEARIFIELD, *Inorg. Chem.* **3** (1964) 146.
24. J. R. SOHN andH. J. JANG, *J. Mol. Catal.* **64** (1991) 349.
25. A. CIMINO, B. A. DEANGELIS, A. LUCHETTI and G. MINELLI, *J. Catal.* **45** (1976) 316.
26. R. MERRYFIELD, M. MCDANIEL and G. PARKS, *J. Catal.* **77** (1982) 348.
27. A. R. GONZALEZ-ELIPE, J. P. ESPINOS, A. FERNANDEZ and G. MANUERA, *Appl. Surf. Sci.* **45** (1990) 103.
28. L. P. HAMMETT and A. J. DEYRUP, *J. Amer. Chem. Soc.* **54** (1932) 2721.
29. F. G. A. OLAH, G. K. S. PRAKASH and J. SOMMER, *Science* **206** (1979) 13.
30. M. ITOH, H. HATTORI and K. TANABE, *J. Catal.* **35** (1974) 225.
31. V. A. DZISKO, Proceedings of the Third International Congress on Catalysis, Vol 1, No. 19, Amsterdam, (1964).
32. M. MIURA, Y. KUBOTA, T. IWAKI, K. TAKIMOTO and Y. MURAOKA, *Bull. Chem. Soc. Jpn.* **42** (1969) 1476.
33. E. P. PARRY, *J. Catal.* **2** (1963) 371.
34. M. C. KUNG and H. H. KUNG, *Catal. Rev. Sci. Engng.* **2** (1985) 425.
35. G. CONNELL and J. A. DUMESIC, *J. Catal.* **105** (1987) 285.

Received 14 April 1992
and accepted 3 February 1993